A New Role of CFD Simulation in Thermal Design of Compact Electronic Equipment: Application of the Build-up Approach to Thermal Analysis of a Benchmark Model

Wataru Nakayama*
ThermTech International,
920-7 Higashi Koiso, Oh-Iso,
Kanagawa 255-0004, Japan
e-mail: WatNakayama@aol.com

Ryuichi Matsuki

Yukari Hacho

Kiyoko Yajima

Shinko Electric Industries Co. Ltd.,
Advanced Product Design & Development Division,
Engineering Department,
80 Oshimada-Cho, Nagano,
Nagano 381-2287, Japan

Computational Fluid Dynamics (CFD) codes have proved their high potential as a tool of thermal design of electronic equipment. However, as the product development cycle is shortened, the CFD-based thermal design needs a new format that allows the packaging designer fast and versatile searches for better design options. The most serious factor that slows the CFD-based design is geometric complexity created by packing various components in a tight space of the system box. In a proposed methodology coined "Build-up Approach (BUA)," CFD simulations are conducted on a set of hardware models to gain insight into the effects of component placement on the junction temperature. Two algorithms are introduced before and after CFD simulations: one defines the geometric parameters through singular value decomposition (SVD) of components placement patterns and the other identifies important geometric parameters by means of the Taguchi method. A case study was conducted on a simple hardware model (benchmark model) that embodies essential features of portable electronic equipment. The results proved the effectiveness of these algorithms in measuring the relative importance of geometric parameters and weeding out unimportant geometric details. [DOI: 10.1115/1.1827259]

Introduction

In various classes of electronic equipment the packaging density in the system box is rapidly rising. This is most visible in portable electronic equipment, such as laptops, cell phones, digital cameras, and other items around us, where an increasing number of functional components are squeezed into an ever-shrinking system box. Compact packaging is also in progress in desktops and server computers, driven by the needs to reduce the box dimensions and cut wiring distances between electronic devices. Components packed in a tight space constitute geometrically complex heat flow paths that pose enormous difficulty to the attempt to perform thermal analysis [1].

In the industry today, Computational Fluid Dynamics (CFD) codes are widely used as a tool of thermal analysis. CFD solutions of high spatial and temporal resolutions can be obtained on a desktop computer or even a laptop. However, CFD-based thermal analysis is not necessarily easy to perform where the object of analysis is geometrically complex. Before embarking on CFD analysis the analyst has to devise a model, omitting some geometric features of structures and approximating complex configurations by simpler ones. This first phase of analysis is an art that often determines the accuracy of the end result no matter how rigorously the subsequent CFD analysis is performed. Although CFD code vendors are providing the tools for the user to set up pre-CFD models and generate meshes, the modeling still remains in the realm of art, increasingly difficult art with the growth of geometric complexity in the system box. Even after some simplifications, the model tends to be complex, reflecting the situation in the actual equipment. The CFD simulation on such a model involves a large number of meshes and, thus, requires a powerful computer and long computing time. Also, the analyst often has to iteratively search for a better mesh system to improve the confidence in the simulation result, and such a search is time consuming where heat transfer paths are complex. So, with the progress of compact packaging, the time and the computational resource required for CFD-based thermal analysis are increasing. On the other hand, the market force demands shorter design time to accelerate product development. It is now an industry-wide concern how to raise the productivity of thermal analysis.

In an attempt to respond to this industrial need a work group is organized under the auspices of the Computational Mechanics Division of the Japan Society of Mechanical Engineers (JSME) [2]. In the group work we are focusing on system-level thermal design of electronic equipment. The basic scheme is to apply information processing techniques on solutions obtained by CFD simulations. The overall organization of the project work is described in earlier publications [2–4]. The present paper first explains the concept of a CFD-based approach to thermal design of complex heat transfer systems, then illustrates the application of the proposed methodology to an equipment model.

Outline of the Build-up Approach

The proposed approach is named the ''Build-up Approach'' (BUA), referring to its hierarchical organization. In Fig. 1, the work organization, divided into the *work level* and the *base level*, is shown with the time axis. The end product is a thermal diagnosis code that provides the packaging designer with a means to quickly grasp the effects of component placement change and other design alterations on the key component temperatures. Such convenience and speed of temperature estimation or diagnosis will be gained by sacrificing the generality of the design code; that is, we focus on a particular class of product, such as a laptop com-

*Corresponding author.
Manuscript received April 25, 2004; revision received April 30, 2004. Review conducted by: B. Sammakia.

HIERARCHICAL ORGANIZATION OF DESIGN ANALYSIS

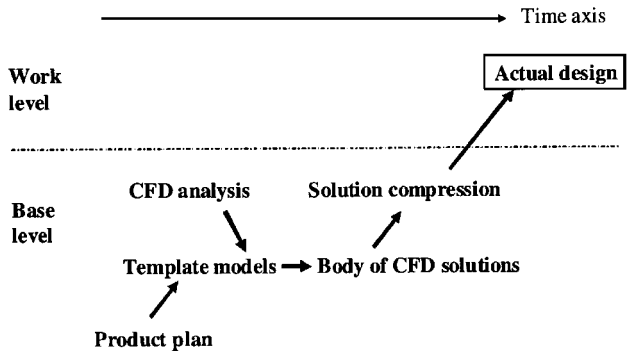

Fig. 1 Proposed hierarchical organization of design work

puter, and develop a code for that product class. We start the process of code development well in advance of the actual design phase. Exploiting a relatively long lead time before the actual design starts, we perform the base level work, as in Fig. 1.

The template model in the BUA is a model that has possible dimensions and physical properties expected in a prospective product design. A set of template models is designed to cover a range of geometric and operative parameters with the intent that we would later locate an actual design point. We perform CFD analysis on the template model set and generate a number of solutions, which constitute a knowledge base. Out of the solution body, in a process termed ''solution compression,'' we scoop up information that is to be incorporated in the diagnosis code.

A plausible format of solution compression is the creation of a thermal resistance network and its resistance values. In this sense, the BUA is an extension of the compact modeling [5] that has been developed for package-level thermal analysis. However, in working on box-level design, we have to deal with a far higher degree of freedom in geometric design than at the package level and need a novel methodology to deal with geometric complexity.

Algorithmic Vehicles of BUA

This section discusses the algorithms employed in the BUA. For template models, a set of component placement patterns are sampled from a number of possible patterns. Sampling has to be done in a systematic fashion, and, for this, geometric patterns need to be represented on a certain code system. The basic idea in the BUA is that a string of binary digits (0,1) or alphabetical symbols is related to the geometric information by a certain rule. The idea was tested in earlier studies. In [6], where the performance of heat spreader plate is studied, the numeral string system is linked to the cut-and-slide operation to generate a number of heat spreader configurations. In [7], where heat conduction through composite slabs is studied, the singular-value-decomposition (SVD) technique is applied to a pattern of conductive elements in a slab, and the eigenvector components of the placement pattern are found. Then, the eigenvector components are represented by alphabetical symbols. Shuffling of the symbols triggers rearrangement of the eigenvectors, resulting in different patterns of conductive elements. In this paper, SVD-based shuffling is also applied to a model of electronic equipment.

Complex geometry means a large number of geometric parameters are to be considered in the analysis. In dealing with many-parameter problems, a strategy is needed to achieve a high efficiency of parameter sampling. The efficiency of sampling is measured by the number of parametric points visited in the analysis to deduce a conclusion about the influence of the parameters on the key component temperatures; the fewer the sampling points, the higher the efficiency. Where the relevant parameters are all quantitative and small in number, the sampling can be coupled with the evaluation of parameter effectiveness in a classical response surface method that leads one to the next sampling points on a maximum gradient path. Where some of the parameters are represented by symbols, either in numeral strings or strings of alphabet letters, we need to resort to non-classical sampling methods. In the BUA we adopt the Taguchi method [8] or the method of experimental design. The original objective of the Taguchi method is to reduce the number of experimental runs that are required to gain insight into the effects of the process parameters on the quality of final products. Attempts to extend the method beyond quality control applications have been reported in the recent literature. For example, the method is applied to the process control of electronic packaging [9,10] and the mechanical reliability analysis of electronic components [11]. A combination of the Taguchi method and the genetic algorithm is employed in thermal analysis and design of composite slabs [7].

The Taguchi method, in its simplest form, samples two points on each parameter (in two-level factorial experimental design). These points are maximum and minimum in an assumed range of the parameter and given labels 1 and 2, respectively. Suppose that we have M parameters and consider the effectiveness of a particular parameter P_1. Suppose also $N\times$CFD runs are performed, setting P_1 at level 1 and other parameters ($P_m, M \geqslant m \geqslant 2$) at either level 1 or 2. We arrange to have other parameters take on levels 1 and 2 at equal frequency in N runs for level 1 of P_1. Hence, the number of 1's and 2's of every parameter other than P_1 are equal to $N/2$. Likewise, conduct $N\times$CFD runs, setting P_1 at level 2 and other parameters at either level 1 or 2, again, in total $N/2$ times each. We average the results, such as the junction temperatures of the CPU chip, from N solutions for level 1 of P_1, so find T_1. Likewise, we find the average T_2 from N solutions for level 2 of P_1. The difference between T_1 and T_2 shows the effect of P_1 on the junction temperature because the effects of all other parameters are likely to be cancelled out in averaging and subtraction. In order to apply the same logic equally to all M parameters, we need to introduce a certain constraint on the number M. For a two-level factorial design, practically, $M=7$, 15, or 31. M larger than 31 makes the plan of CFD run unwieldy.

There is another fundamental constraint accompanying the above logic for deducting the parameter effects. The logic is based on an assumption that the contributions from the parameters to the result are linear; that is, the change of level in one parameter does not affect the effects of other parameters on the result. Where we have strong nonlinear dependency among the parameters, we need additional algorithms to gauge the effects of interactive working of the parameters. In the example described later, such nonlinear effects are assumed to be weak.

Once we develop the body of CFD solutions, we estimate the effects of parameters on the temperature of key components. (Later, we will use the thermal resistance instead of temperature.) The evaluation steps in the Taguchi method are summarized as follows. Suppose that eight CFD runs are performed, setting seven parameters in a two-level factorial table; that is, $M=7$ and $2N=8$. Sampled levels are projected in the table where the CFD run numbers (k) enter the leftmost column, and the parameter symbols in the uppermost row, see an actual Table 3(b) in the later section. From the CFD solutions we find eight thermal resistance values, $\theta_{ja,k}\,(1\leqslant k\leqslant 8)$ for a set of seven parameters, $P_m\,(1\leqslant m\leqslant 7)$. The level of P_m is denoted by $P_m=1$ or 2.

Step 1: Compute the column average,

$$\overline{\theta}=\frac{1}{8}\sum_{k=1}^{8}\theta_{ja,k}. \tag{1}$$

Step 2: Compute the deviation from the column average for $\theta_{ja,k}$ of each run

$$\Delta\theta_{ja,k}=\theta_{ja,k}-\overline{\theta}. \tag{2}$$

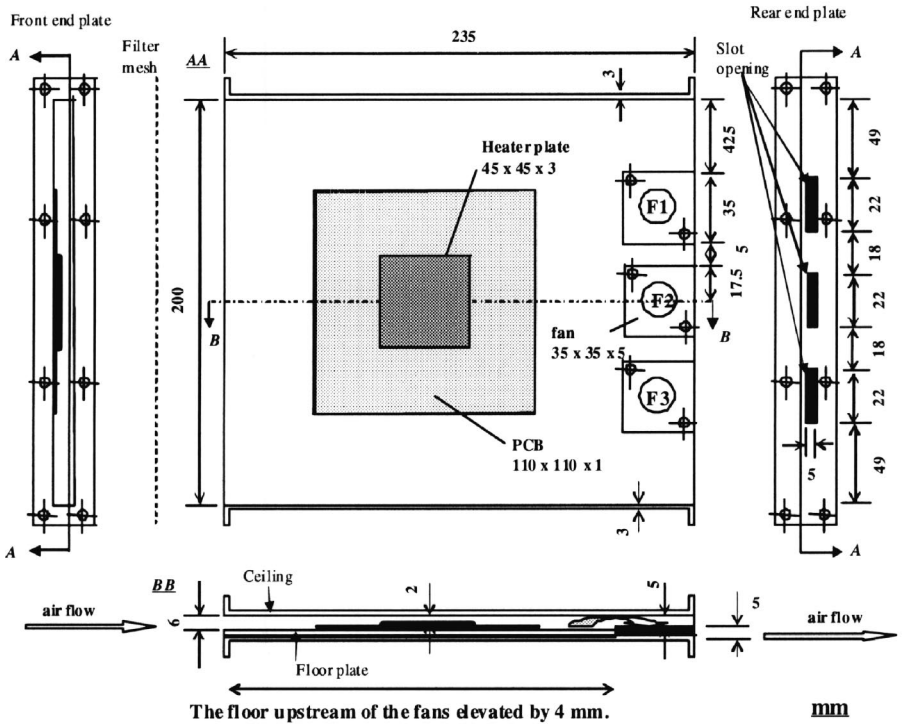

Fig. 2 Benchmark model

Step 3: The effect of P_m on θ_{ja} is computed as

$$S_m = \frac{[(average\ \Delta\theta_{ja,k} \quad \text{for } P_m = 1) - (average\ \Delta\theta_{ja,k} \quad \text{for } P_m = 2)]^2}{8 \times (\frac{1}{4})^2}, \tag{3}$$

where "average $\Delta\theta_{ja,k}$ for $P_m = 1$ (or 2)" means the average taken over those $\Delta\theta_{ja,k}$ from CFD runs where parameter P_m is set at 1 (or 2) while other parameters occur at levels 1 and 2 at equal frequency (i.e., twice at each level). The denominator on the right-hand side is a factor introduced to account for the data population involved in the computation. Because it is cancelled out in later computations, the detailed account about this factor is omitted.

Step 4: Contribution from P_m to θ_{ja} is computed as

$$\rho_m = S_m \Big/ \sum_{m=1}^{7} S_m . \tag{4}$$

Equations (1)–(4) are the basic steps of evaluation. More information can be obtained by analyzing the CFD results from different angles, such as whether or not nonlinear interactions are involved. There are commercial software codes that assist in the development of a table of parametric levels and the evaluation of results. For the present example study, we used a code DESIGN DIRECTOR PLUS, developed by NHK [12].

Benchmark Model

In the JSME project, we work on a hardware model, the structural organization of which is not overly complex but retains some essential features of compact electronic equipment. The model can be used to benchmark the result of CFD simulation and is, hence, called the benchmark model. Figure 2 shows the model used in the present work, which is composed of a system box, heater plate, a printed cardboard (PCB), several dummy blocks, and three fans.

The internal space of the system box is 200 mm wide, 235 mm long, and 10 mm high. A 4 mm thick acrylic floor plate is placed on the floor area 200 mm×200 mm, narrowing the height of airflow space upstream of the fans to 6 mm. The heat source is a heater plate (hereafter referred as "Heater") bonded on the PCB. The footprint area of Heater is 45 mm×45 mm, and the thickness is 3 mm (including the thickness of interface to PCB). The Heater is composed of two copper plates sandwiching a sheet heater. The PCB has an area 110 mm×110 mm, and is 1 mm thick. When PCB is bonded to the floor plate, a 2 mm high air space is left between Heater and the underside of the box ceiling. In addition to Heater/PCB, there are non-heat dissipating (dummy) blocks placed on the floor plate. They are not included in Fig. 2, but will be shown in the subsequent figures. Two types of dummy blocks are employed; one (designated by symbol D1) has a footprint area 45 mm×45 mm and a thickness 5 mm, and the other (D2) has the dimensions 20 mm×20 mm×3 mm. The placement pattern of Heater/PCB and the dummy blocks on the floor plate is the geometric parameter of interest in this study. The next section explains how the pattern is represented by symbols.

Three fans are screwed to the box floor at the right end of the box. The fan is a flat-type, which sucks air from the top and discharges from the side. The fan locations are designated by symbols F1, F2, and F3. The fans are operated individually, and, hence, a combination of active fans is one of the parameters; that is, the active fan is F1, F2, or F3 in the one-fan operation, the active fans are (F1, F2), (F2, F3), or (F3, F1) in the two-fan operation, or all three fans are activated.

The PCB has two heat-spreader copper layers. The heat-spreader copper is 0.03 mm thick and covers most of the PCB

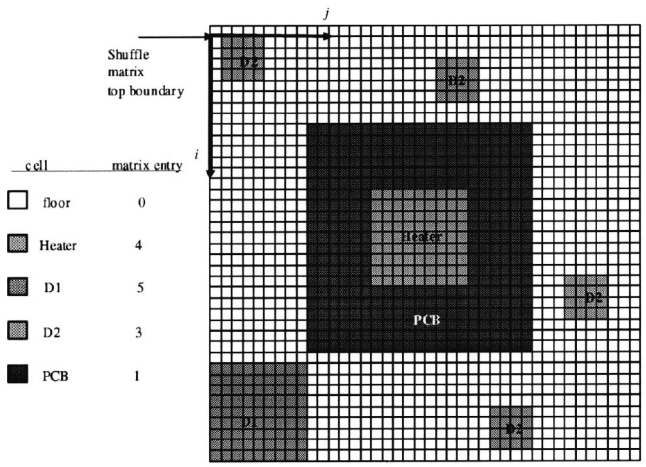

Fig. 3 Eight placement patterns corresponding to the two-level factorial table [Table 3(b)]box

area. The signal copper is laid out in narrow strips on the top surface of PCB, therefore, it has insignificant effect on heat spreading.

Generation of Template Models From the Benchmark Model

We start working with a sample placement pattern (starter pattern), shown in Fig. 3. Figure 3 shows only the area for components placement (shuffling area). This starter pattern has Heater/PCB at the center of the shuffling area, one dummy block D1, and four D2 blocks. In the present model the fan locations are symmetric with respect to the horizontal centerline. This fan arrangement is used to narrow down the areas for placement of the Heater/PCB and D1. The Heater/PCB is moved in the upper section of the floor, and D1 is moved only in the lower section. While D1 is allowed to touch the side wall, PCB and D2 are not. Hence, the area of actual shuffling is defined from the bottom to the upper line marked by ''Shuffle matrix top boundary.''

The shuffling area is discretized into 39×40 cells, and the row/column numbering system (i,j) is introduced. Note that the airflow moves in the direction of increasing j. We consider a matrix **S** composed of component heights. For open cells whose area is free of any component, 0 is entered as the matrix element; 3 is entered in $\{1\leqslant i\leqslant 4,2\leqslant j\leqslant 5\}$, which is the location of one of the D2 blocks in the upper-left corner; 1 in $\{9\leqslant i\leqslant 29,10\leqslant j\leqslant 15\}$, $\{9\leqslant i\leqslant 29,25\leqslant j\leqslant 30\}$, $\{9\leqslant i\leqslant 14,16\leqslant j\leqslant 24\}$, $\{24\leqslant i\leqslant 29,16\leqslant j\leqslant 24\}$, the cells covered by PCB (excluding the central area covered by Heater); 4 in $\{15\leqslant i\leqslant 23,16\leqslant j\leqslant 24\}$, the cells covered by Heater; and so on. The matrix **S** is then decomposed into the left-singular matrix **U** and the right-singular matrix **V** [13],

$$\mathbf{S}=\mathbf{U}\Sigma\mathbf{V}^{\mathbf{T}} \tag{5}$$

where

$$\Sigma=\begin{bmatrix} \sigma^{(1)} & 0 & \cdot & \cdot & & \cdot & 0 \\ 0 & \sigma^{(2)} & \cdot & \cdot & \cdot & \cdot & \cdot \\ \cdot & \cdot & \cdot & \cdot & \cdot & \cdot & \cdot \\ \cdot & \cdot & \cdot & \cdot & \cdot & \cdot & 0 \\ 0 & \cdot & \cdot & \cdot & \cdot & 0 & \sigma^{(K)} \end{bmatrix} \tag{6}$$

$\sigma^{(k)}=\sqrt{\lambda^{(k)}}$, and $\lambda^{(k)}$ is the kth eigenvalue. Refer to [7,13] for the method to determine the eigenvalues and the singular matrixes **U** and **V**. For the sample pattern of Fig. 4, there are seven eigenvalues, **U** is a matrix composed of 39 rows and 7 columns, and **V** has 40 rows and 7 columns. Note that $\mathbf{V}^{\mathbf{T}}$ in Eq. (5) is the transpose of **V**, so that matrix multiplication on the right-hand side produces a 39×40 matrix (that is **S**).

Examination of **U** and **V** reveals that some rows are repeated, hence, the actual number of distinct rows is 10 in **U** and 9 in **V**. These distinct rows in **U** are represented by symbols x_0-x_9, and those in **V** by y_0-y_8. Table 1 shows the list of eigenvalues and the building blocks of **U** and **V**. Table 2 shows the arrangement and further grouping of symbols. The arrangements of building blocks in Table 2(a) reproduce the starter pattern of Fig. 3; that is, **U** and **V** having these building block arrangements and Σ of $\sigma^{(k)}$ $[=\sqrt{\lambda^{(k)}}$ from Table 1] produce the starter pattern. Now, we shuffle the building blocks, so, permute rows in **U** and also rows in **V**. Substitution of these changed **U** and **V** in Eq. (5), using the same Σ, results in a different **S**, hence, a different cell placement pattern on the floor plate. Further shuffling creates various patterns. We need to maintain the configurations of the components during shuffling. This requirement is met by grouping the building blocks as shown in Table 2(*b*). For example, group X_2 is composed of $9\times x_4$, $8\times x_5$, x_6, $3\times x_7$, and Y_2 composed of $7\times y_3$, $6\times y_4$, $3\times y_5$, y_6, $4\times y_7$. These groupings are necessary to maintain the configuration of Heater/PCB, though X_2 and Y_2 can be moved individually. The building blocks within the group

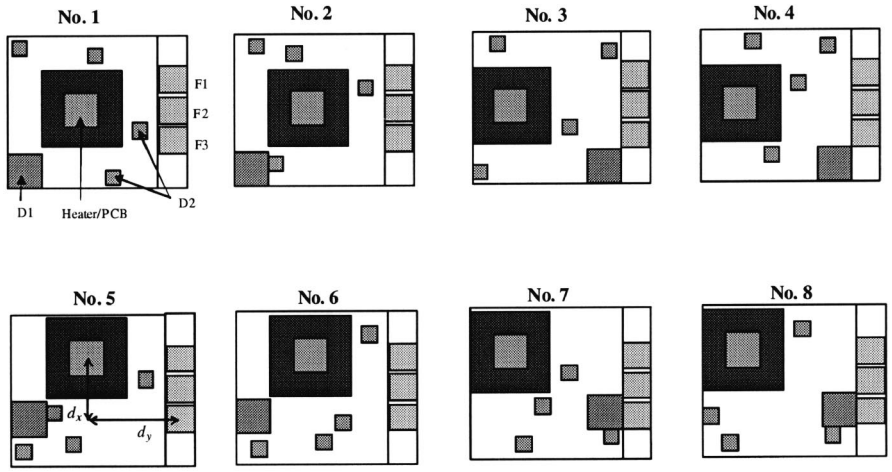

Fig. 4 Starter pattern of component placement in the system

Table 1 Eigenvalues and building block elements of left-singular vectors matrix U and right-singular vectors matrix V derived from a sample components placement

Eigenvalues							
$\lambda^{(1)}=2.1726\times10^{3}$							
$\lambda^{(2)}=1.6321\times10^{3}$							
$\lambda^{(3)}=1.6359\times10^{2}$							
$\lambda^{(4)}=1.3055\times10^{2}$							
$\lambda^{(5)}=8.6673\times10^{1}$							
$\lambda^{(6)}=4.3906\times10^{1}$							
$\lambda^{(7)}=2.7607\times10^{1}$							
Building blocks for **U**							
x_0:	0	0	0	0	0	0	0
x_1:	8.6319×10^{-2}	1.7710×10^{-2}	1.4194×10^{-1}	1.7243×10^{-1}	2.1210×10^{-2}	5.2459×10^{-1}	6.2456×10^{-3}
x_2:	9.9413×10^{-2}	-6.2516×10^{-2}	3.5054×10^{-1}	4.0678×10^{-1}	1.5986×10^{-1}	6.8064×10^{-2}	3.1765×10^{-2}
x_3:	1.3094×10^{-2}	-8.0226×10^{-2}	2.0860×10^{-1}	2.3434×10^{-1}	1.3865×10^{-1}	-4.5653×10^{-1}	2.5520×10^{-2}
x_4:	2.0955×10^{-2}	-9.6320×10^{-2}	-7.4192×10^{-2}	-3.6040×10^{-3}	1.6289×10^{-1}	1.7421×10^{-2}	-2.4733×10^{-1}
x_5:	4.8949×10^{-2}	-3.0119×10^{-1}	7.2067×10^{-2}	-1.1463×10^{-1}	-3.2629×10^{-2}	2.1067×10^{-2}	4.5710×10^{-2}
x_6:	5.0934×10^{-2}	-3.1547×10^{-1}	-2.0453×10^{-1}	2.2120×10^{-1}	-3.1901×10^{-1}	-5.3071×10^{-3}	2.6107×10^{-1}
x_7:	2.2940×10^{-2}	-1.1060×10^{-1}	-3.5079×10^{-1}	3.3222×10^{-1}	-1.2349×10^{-1}	-8.9531×10^{-3}	-3.1973×10^{-2}
x_8:	3.1087×10^{-1}	7.0529×10^{-2}	8.0704×10^{-2}	-1.8863×10^{-2}	-2.3383×10^{-1}	-5.7535×10^{-2}	-1.8311×10^{-1}
x_9:	3.3708×10^{-1}	4.5714×10^{-2}	-1.5187×10^{-1}	-5.6386×10^{-2}	2.4563×10^{-1}	-9.9093×10^{-3}	2.1820×10^{-1}
Building blocks for **V**							
y_0:	0	0	0	0	0	0	0
y_1:	3.1137×10^{-1}	6.6276×10^{-2}	-7.9740×10^{-2}	-1.3997×10^{-1}	-1.0024×10^{-1}	-2.4699×10^{-1}	-4.0672×10^{-2}
y_2:	3.3528×10^{-1}	5.9622×10^{-2}	1.5129×10^{-1}	1.6419×10^{-1}	1.6455×10^{-2}	2.8967×10^{-1}	2.7346×10^{-3}
y_3:	1.5017×10^{-2}	-9.7123×10^{-2}	-1.0540×10^{-1}	2.3490×10^{-2}	5.5369×10^{-2}	4.4244×10^{-2}	-3.2263×10^{-1}
y_4:	4.3499×10^{-2}	-2.9948×10^{-1}	-1.8148×10^{-2}	-1.5920×10^{-1}	-1.3154×10^{-1}	1.1815×10^{-1}	3.5221×10^{-2}
y_5:	5.7982×10^{-2}	-3.2068×10^{-1}	2.4415×10^{-1}	1.7746×10^{-1}	6.0839×10^{-2}	-2.3361×10^{-1}	1.0064×10^{-1}
y_6:	2.9499×10^{-2}	-1.1832×10^{-1}	1.5690×10^{-1}	3.6015×10^{-1}	2.4775×10^{-1}	-3.0751×10^{-1}	-2.5722×10^{-1}
y_7:	1.0180×10^{-1}	-8.3544×10^{-2}	-2.4789×10^{-1}	-3.5729×10^{-2}	3.7197×10^{-1}	2.6298×10^{-2}	1.7571×10^{-1}
y_8:	7.7076×10^{-3}	-4.8065×10^{-2}	-2.9482×10^{-1}	3.1976×10^{-1}	-2.2218×10^{-1}	-1.4563×10^{-2}	9.4296×10^{-2}

can be rearranged under certain constraints. For X_1, for example, $2\times x_1$ and $2\times x_3$ can be exchanged, and we have two variants of X_1, X_{11} and X_{12}, as shown in Table 2(*b*). This is a reflection operation that switches two D2 dummy components in the upper region with respect to their vertical locations. That is, by going from X_{11} to X_{12}, D2 in the upper left corner shifts down by two notches, and another D2 moves up by two notches. A constraint in this case is that $(x_1\,x_1)$ and $(x_3\,x_3)$ are switched holding $(x_2\,x_2)$ in the middle, otherwise, the integrity of either one or both of D2 blocks is spoiled. Similarly, we perform only reflection operations on other groups (from X_2 to Y_2), and generate two offspring as shown in Table 2(*b*) (from X_{21} to Y_{22}). The rows of all zero elements, (x_0) and (y_0), are spacers, and, in subsequent discussion, they are represented by symbols X_0 and Y_0, respectively.

Using these group symbols we define geometric parameters and their levels. Table 3(*a*) shows them; *A* and *B* define the arrange-

Table 2 Symbolic representations of building block arrangements

(*a*) Building block arrangements of starter pattern (Case No. 1)

For left-singular matrix **U**

$x_1\,x_1\,x_2\,x_2\,x_3\,x_3\,x_0\,x_0\,x_4\,x_4\,x_4\,x_4\,x_4\,x_4\,x_5\,x_5\,x_5\,x_5\,x_5\,x_5\,x_5\,x_5\,x_6\,x_7\,x_7\,x_7\,x_4\,x_4\,x_4\,x_0\,x_8\,x_8\,x_8\,x_8\,x_9\,x_9\,x_9\,x_9\,x_8$

For right-singular matrix **V**

$y_1\,y_2\,y_2\,y_2\,y_2\,y_1\,y_1\,y_1\,y_3\,y_3\,y_3\,y_3\,y_3\,y_3\,y_4\,y_4\,y_4\,y_4\,y_4\,y_4\,y_5\,y_5\,y_5\,y_6\,y_3\,y_7\,y_7\,y_7\,y_7\,y_0\,y_0\,y_0\,y_8\,y_8\,y_8\,y_8\,y_0\,y_0\,y_0$

(*b*) Groups of building blocks

Group symbol	Constituents
X_1	$2\times x_1$, $2\times x_2$, $2\times x_3$
X_2	$9\times x_4$, $8\times x_5$, x_6, $3\times x_7$
X_3	$5\times x_8$, $4\times x_9$
X_0	x_0
Y_1	$5\times y_1$, $4\times y_2$
Y_2	$7\times y_3$, $6\times y_4$, $3\times y_5$, y_6, $4\times y_7$
Y_3	$4\times y_8$
Y_0	y_0
Internal organization variants: only reflections	
Symbol	Arrangement
X_{11}	$x_1\,x_1\,x_2\,x_2\,x_3\,x_3$
X_{12}	$x_3\,x_3\,x_2\,x_2\,x_1\,x_1$
X_{21}	$x_4\,x_4\,x_4\,x_4\,x_4\,x_4\,x_5\,x_5\,x_5\,x_5\,x_5\,x_5\,x_5\,x_5\,x_6\,x_7\,x_7\,x_7\,x_4\,x_4\,x_4$
X_{22}	$x_4\,x_4\,x_4\,x_7\,x_7\,x_7\,x_6\,x_5\,x_5\,x_5\,x_5\,x_5\,x_5\,x_5\,x_5\,x_4\,x_4\,x_4\,x_4\,x_4\,x_4$
X_{31}	$x_8\,x_8\,x_8\,x_8\,x_9\,x_9\,x_9\,x_9\,x_8$
X_{32}	$x_8\,x_9\,x_9\,x_9\,x_9\,x_8\,x_8\,x_8\,x_8$
Y_{11}	$y_1\,y_2\,y_2\,y_2\,y_2\,y_1\,y_1\,y_1\,y_1$
Y_{12}	$y_1\,y_1\,y_1\,y_1\,y_2\,y_2\,y_2\,y_2\,y_1$
Y_{21}	$y_3\,y_3\,y_3\,y_3\,y_3\,y_3\,y_4\,y_4\,y_4\,y_4\,y_4\,y_4\,y_5\,y_5\,y_5\,y_6\,y_3\,y_7\,y_7\,y_7\,y_7$
Y_{22}	$y_7\,y_7\,y_7\,y_7\,y_3\,y_6\,y_5\,y_5\,y_5\,y_4\,y_4\,y_4\,y_4\,y_4\,y_4\,y_3\,y_3\,y_3\,y_3\,y_3\,y_3$

Table 3 Definition of geometric parameter levels and two-level factorial table

(*a*) Definition of levels: for groups, cycle rotation; for internal organizations, reflections

Geometric parameter	Level 1	Level 2
A	$X_1\,X_0\,X_0\,X_2\,X_0\,X_3$	$X_2\,X_0\,X_3\,X_1\,X_0\,X_0$
B	$Y_1\,Y_2\,Y_0\,Y_0\,Y_0\,Y_3\,Y_0\,Y_0\,Y_0$	$Y_2\,Y_0\,Y_0\,Y_0\,Y_3\,Y_0\,Y_0\,Y_0\,Y_1$
A_1	X_{11}	X_{12}
A_2	X_{21}	X_{22}
A_3	X_{31}	X_{32}
B_1	Y_{11}	Y_{12}
B_2	Y_{21}	Y_{22}

(***b***) **Two-level factorial table**

Case No.	A	B	A_1	A_2	A_3	B_1	B_2
1	1	1	1	1	1	1	1
2	1	1	1	2	2	2	2
3	1	2	2	1	1	2	2
4	1	2	2	2	2	1	1
5	2	1	2	1	2	1	2
6	2	1	2	2	1	2	1
7	2	2	1	1	2	2	1
8	2	2	1	2	1	1	2

ments of groups X_0-X_3 and Y_0-Y_3, respectively; A_1-B_2 define the internal organizations of X_1-X_3 and Y_1-Y_3. When all the parameters take level 1, the matrix multiplication on the right-hand side of Eq. (5) results in the starter pattern of Fig. 3. Level 2 for A is created by rotating the symbol array by three notches and placing X_2 on the lead and X_0 on the tail. Level 2 for B is created by shifting the array by one notch, placing Y_2 on the lead and Y_1 on the tail. Level 2 for A_2-B_2 is defined by reflected internal organizations of $X_{11}-Y_{21}$.

Table 3(*b*) specifies the geometric parameter levels for eight cases of components placement. Case No. 1 is the starter pattern. Other placement patterns are shown in Fig. 4, where three blocks on the right edge of the floor represent the fans F1, F2, and F3. For each placement case, there are seven cases of fan operation: the active fan is F1, F2, or F3 in the one-fan operation; the active fans are (F1,F2), (F2,F3), or (F3,F1) in two-fan operation; or all three fans are activated. Therefore, in total, 56 CFD runs were performed.

CFD Simulations and Results

The air space, Heater, and PCB are discretized into 144,000–147,000 meshes. The mesh population was varied in this range in order to tailor the discretization for different component placement patterns. The fan curve supplied by the fan vendor is approximated by a line that connects the two extreme points of choked (80 Pa, 0 m^3/min) and open (0 Pa, 0.026 m^3/min) states. The operation point was found close to the open state, where the fan curve is least affected by the presence of solid objects upstream of the fan. The commercially available code FLOTHERM® (supplied by Flomerics, Inc.) was used. Flotherm provides four turbulence models, among them, *Automatic Algebraic*, designated as the default, was used in the present simulations. Checks were made regarding the sensitivity of the solution to the option of the turbulence model by using the standard k-ε model, and the sensitivity was found insignificant. Also, laminar flow simulations were performed by another party to obtain backup checks. Again, the conclusions reported later in the paper were unaltered. Table 4 shows the thermal conductivity of materials constituting the Heater/PCB. Other details involved in the CFD simulations, such as the mesh layout, mesh sensitivity check, and the convergence check, are saved from descriptions here because our focus is on the effects of geometric variations on cooling the Heater.

Table 4 Thermal conductivity of materials contained in Heater/PCB

Material	Component or zone	Thermal conductivity W/m K
Copper	Heater, Copper in PCB	398
FR4	PCB	0.38
Copper/FR4 composite	Through-hole section of PCB	7.7 in plane[a]
		3.6 across[a]
Adhesive[b]	Heater/PCB interface	1.3

[a]Equivalent thermal conductivity was estimated by separate analysis. For the zone other than the through-hole section, copper and FR4 are individually accounted for.
[b]Estimated thickness is 1 mm.

From the CFD solutions, we find maximum Heater temperature ["junction temperature" T_j(°C)] for a specified heat dissipation rate of Heater [Q (W)] and an air temperature at the inlet [T_0(°C)]. The results are reduced to the junction-to-air thermal resistance

$$\theta_{ja}=\frac{T_j-T_0}{Q}\ \text{(K/W)} \tag{7}$$

Figure 5 shows the thermal resistance values in the one-fan operation. Three bars for each template case show the thermal resistances corresponding to active fan locations, from left to right, F1, F2, and F3. Variations of thermal resistance reflect the effects of the geometric parameters and the active fan location. From cases 1 to 4, the thermal resistance shows small dependence on the fan location, while from cases 5 to 8, the thermal resistance is sensitive to the fan location. Figure 6 shows the thermal resistance in the three-fan operation. It is noteworthy that the thermal resistances for cases 1, 2, 5, and 6 are distinctly lower than those for cases 3, 4, 7, and 8.

Substituting the results into Eqs. (1)–(4), we compute the contributions of the geometric parameters to the variation of thermal resistance, as shown in Fig. 7. The parameters are those defined in Table 3. The subscript m to ρ of Eq. (4) is now interpreted as any of the parameter symbols from A to B_2. Contributions are plotted in Fig. 7 for all cases of fan operation. The bars, from left to right in each bracket of active fan(s), show the contributions from parameters $A\sim B_2$. In the one-fan operation, parameter A has the highest contribution, followed by parameter B. In the two-fan operation, parameter B is the most influential, whereas parameter A also makes some contributions in cases F1/F2 and F2/F3. In the three-fan operation, parameter B is an outstanding contributor. In all cases of fan operation, parameters A_1-B_2 have insignificant contributions.

Interpretation of the results about thermal resistance and parameter contribution is now presented referring to Table 3(*b*) and Fig. 4. For convenience of discussion we define the terms regarding the relative distance between Heater/PCB and the active fan as follows. The center-to-center separation between Heater/PCB and the fan is defined in terms of the cross-stream distance d_x and the streamwise distance d_y. In Fig. 4, these distances are depicted for case 5 assuming that F3 is active. Two levels of parameter A distinguish the cross-stream location of Heater/PCB; at level 1 (cases 1–4), the Heater/PCB is on the centerline of the box, and at level 2 (cases 5–8) it is displaced toward the sidewall of the box. In the one-fan operation, the Heater/PCB at level 2 placement is closest in d_x to the active fan when F1 is active and farthest from the active fan when F3 is active. Large variations in the thermal resistance for cases 5–8 in Fig. 5 reflect the effects of d_x on heat transfer from the displaced Heated/PCB. On the other hand, the thermal resistances for cases 1–4 in Fig. 5 show small variations, due to small changes in d_x, where the Heater/PCB is placed on the centerline. When collectively seen, the bars for F1 of 1–4 are taller than those of cases 5–8. The bar-heights for F2 active of 1–4 are generally less than those of cases 5–8, and this becomes

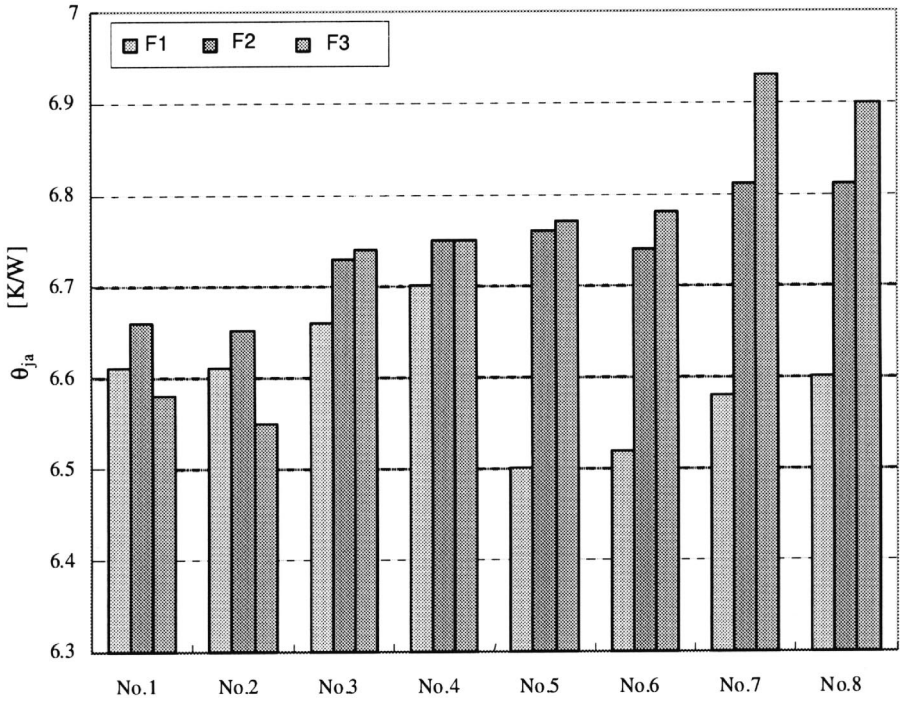

Fig. 5 Thermal resistances for eight placement patterns: the cases of one-fan operation

more obvious when F3 is active. High sensitivity of the thermal resistance to the cross-stream location of the Heater/PCB is reflected in the largest contributions from parameter *A* in the one-fan operation as seen in Fig. 7.

Parameter B accounts for the streamwise location of the Heater/PCB; at level 1 (cases 1, 2, 5, 6), it is in the middle; and at level 2 (cases 3, 4, 7, 8), it is moved toward the inlet of the box. Interpretation of the combined effect of parameters *A* and *B* is attempted below, referring to the airflow streamlines in the box.

Two samples of airflow patterns are shown in Fig. 8: (*a*) shows streamlines for the case of minimum d_x and d_y (case 5 with F1 active) and (*b*) for the case of maximum d_x and d_y (case 8 with F3 active). The number of streamlines over the Heater is almost equal in both figures, but those in Fig. 8(*a*) show convergence near the downstream end of the Heater. Although the streamline convergence appears small, it actually has the effect of increasing the volumetric average of air velocity in the space between the Heater of case 5-F1 and the box ceiling more than 100% over that of case

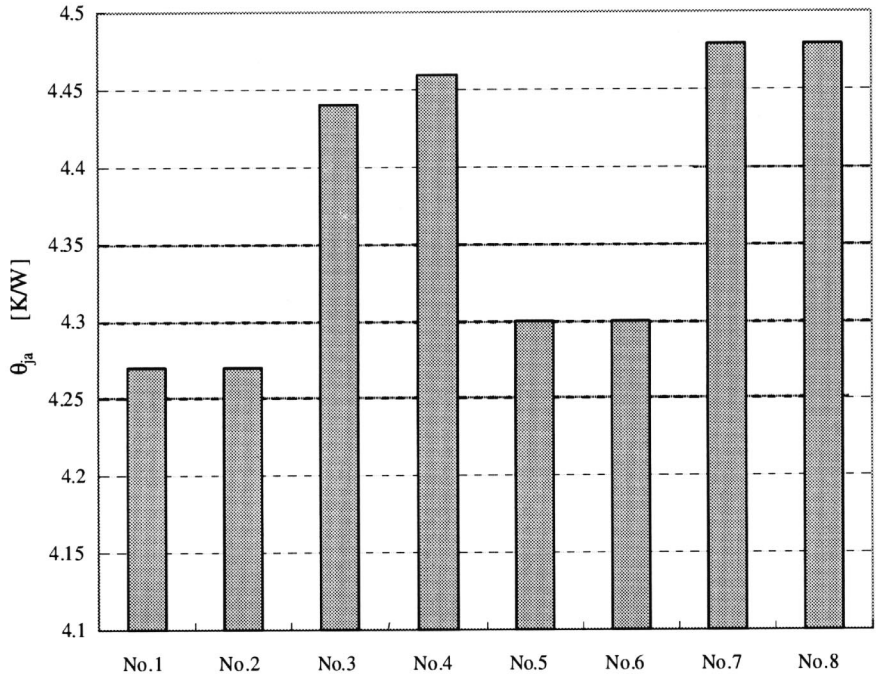

Fig. 6 Thermal resistances for eight placement patterns: the cases of three-fan operation

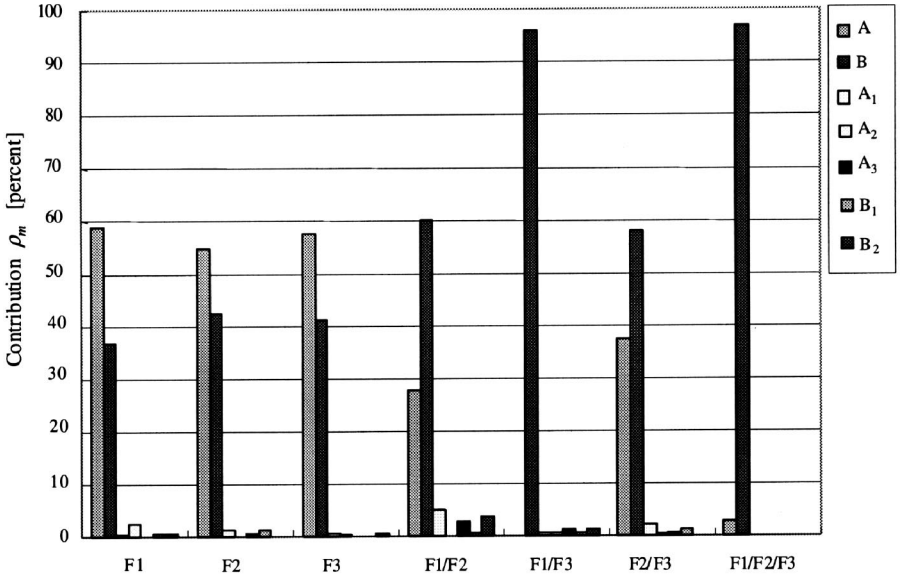

Fig. 7 Contributions from geometric parameters ($A \sim B_2$) to thermal resistance variations caused by shuffling of the components in the system box: the cases of one-fan operation (F1,F2,F3), two-fan operation (F1/F2,F1/F3,F2/F3), and three-fan operation (F1/F2/F3)

8-F3 (0.12 m/s versus 0.051 m/s). Also, in case 5-F1, the streamlines over the downstream part of the PCB are converged because of the proximity of the Heater/PCB to the active fan. The examination of heat flow distributions indicates that about 35% of heat dissipation from the Heater is conducted to the PCB; hence, the streamline convergence over the PCB has some effect on lowering the thermal resistance in case 5-F1.

As the number of active fans is increased, air suction at the end of the box becomes more uniformly distributed. It is plausible that the cross-stream location of Heater/PCB is less relevant to airflow rate over the Heater, and parameter *A* loses its significance. Instead, parameter *B*, in other words, the streamwise distance d_y, comes to have a dominant effect on the airflow. In Fig. 7, the dominant effect of parameter *B* is most obvious when F1 and F3 are active in two-fan operation and all fans are active. Figure 6 shows clear distinction between the thermal resistances of the two groups, one of cases 1, 2, 5, and 6, and the other of cases 3, 4, 7, and 8. Close examination of the solutions reveals that the airflow rate over the Heater becomes less when the Heater/PCB is at the inlet edge than when it is in the middle of the box.

Minor contributions from parameters $A_1 - B_2$ to the thermal resistance are manifestations of the fact that detailed placement patterns of dummy components are mostly irrelevant to the determination of thermal resistance. Practical significance of such a finding is obvious. In an actual case of component placement design, following the steps described above, some components will be identified as having insignificant influence on the junction temperature. Therefore, the precise location of those components does not have to be taken into account in the CFD analysis. An additional CFD run is not necessary when those components are relocated in the course of hardware design. The effect of such insignificant components on airflow may be captured as a lump flow resistance in front of the box, or it may be neglected altogether if it is small. In a further study on component location in the system box, only those components of significance are left in a CFD model. The saving of analysis time is gained by simplification of the geometry.

Conclusions

The CFD code allows one to find detailed temperature and airflow distributions inside the system box of electronic equipment. A substantial part of the knowledge produced by CFD simulations is unobtainable by experimental measurements, and detailed three-dimensional pictures of the temperature field on the computer display or in print are reassuring to the packaging designer. However, in an exercise of design judgement, only condensed information suffices, such as that which relates the temperatures of key components to the environment (air) temperature in terms of thermal resistance. Instead, the relationship between thermal resistance and the various options of component placement in the system box is a matter of concern, particularly so in the design of portable and other compact electronic equipment. As a tool to navigate through various design options, the CFD code is inefficient. In a scheme proposed in the present paper, CFD simulations are given a role of developing a knowledge base through coupling with the algorithms that aid navigation in the multidimensional parametric domain. The method was applied to the thermal analysis of a simplified hardware model (benchmark model) having a simulated package (Heater), a printed cardboard (PCB), dummy blocks, and three small fans in a flat system box. From singular value decomposition of a starter placement pattern of the components the geometric parameters and their levels were defined. Then, eight patterns of components placement were created in correspondence with the two-level factorial table of the Taguchi method. CFD simulations were performed on these patterns, and the thermal resistance solutions were subjected to a test to measure contributions from the geometric parameters. An important identified parameter includes the location of the Heater/PCB assembly, in agreement with physical interpretations. The present work paves the way to deal with more geometrically complex systems of actual electronic equipment.

Acknowledgments

The present study is a part of the project ''RC202 Studies on Reliability of Electronic Devices/Electronic Packaging'' that was organized under the auspices of the Computational Mechanics Division, of the Japan Society of Mechanical Engineers. The author is grateful for the support rendered through this JSME project. The authors thanks Kazumasa Fujioka, of Hitachi, Ltd., for his backup work to this study.

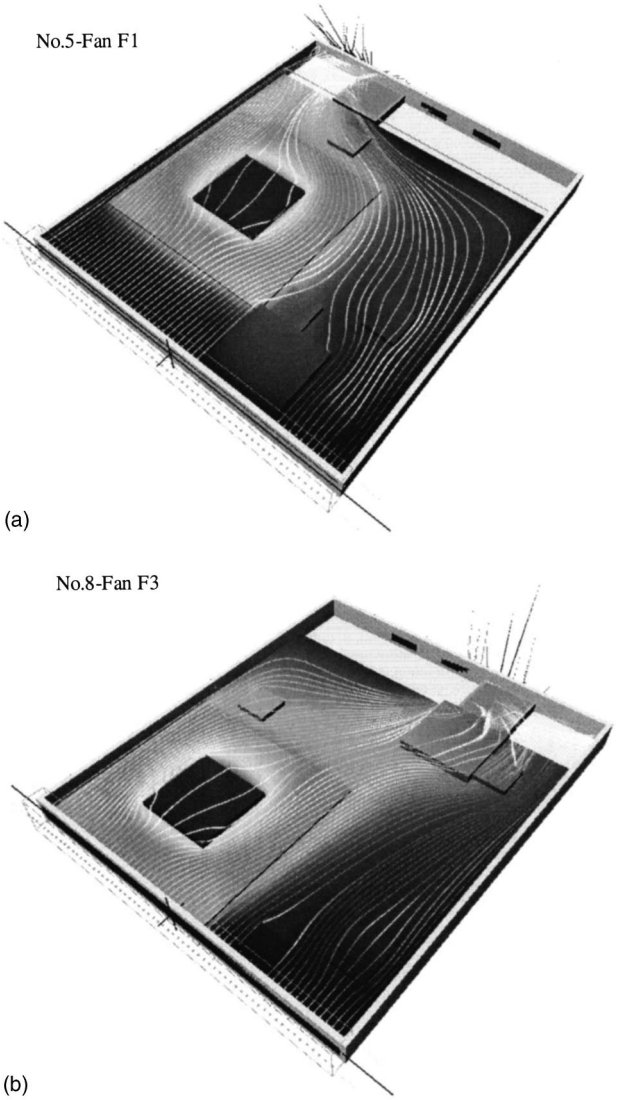

Fig. 8 Airflow streamlines in the system box: (a) The case where Heater/PCB is located closest to the active fan (placement No. 5 and the fan at F1 active); (b) the case where Heater/PCB is located farthest from the active fan (placement No. 8 and the fan at F3 active)

Nomenclature

A = geometric parameter that defines row elements placement in **U** (Table 3)
B = geometric parameter that defines column elements placement in **V** (Table 3)
D1 = dummy block (45 mm×45 mm×5 mm)
D2 = dummy block (20 mm×20 mm×3 mm)
d_x = center-to-center cross-stream distance between Heater/PCB and the active fan
d_y = center-to-center streamwise distance between Heater/PCB and the active fan
F1∼F3 = fan slot
i = cross-stream cell coordinate (Fig. 3)
j = stream-wise cell coordinate (Fig. 3)
M = total number of parameters
N = half the total number of CFD runs
P = geometric parameter
Q = heat flow (W)
$\mathbf{S}$ = matrix composed of component heights
S_m = measure of the effect of parameter P_m (or P_m being any of A, B, A_1-A_3, B_1, B_2) on the thermal resistance [Eq. (3)]
T = temperature (°C)
T_j = maximum heater (''junction'') temperature (°C)
T_0 = air temperature at the inlet of the box (°C)
$\mathbf{U}$ = matrix composed of left-singular vector elements
$\mathbf{V}$ = matrix composed of right-singular vector elements
$\mathbf{V^T}$ = transpose of $\mathbf{V}$
X = row element group
x = building block row element of $\mathbf{U}$
Y = column element group
y = building block row element of $\mathbf{V}$

Greek Symbols.

$\lambda^{(k)}$ = kth eigenvalue
θ_{ja} = junction-to-air thermal resistance (K/W) [Eq. (7)]
$\bar{\theta}$ = column average of θ_{ja} (K/W) [Eq. (1)]
$\Delta\theta_{ja,k}$ = deviation of $\theta_{ja,k}$ from the column average (K/W) [Eq. (2)]
ρ_m = contribution of parameter P_m (or P_m being any of A, B, A_1-A_3, B_1, B_2) to the thermal resistance [Eq. (4)]
Σ = matrix composed of $\boldsymbol{\sigma}^{(k)}$ and 0 [Eq. (6)]
$\boldsymbol{\sigma}^{(k)}$ = square root of $\lambda^{(k)}$

Subscripts.

k = kth CFD simulation run
m = mth parameter
0 = spacer cell (the floor cell not covered by any component)
1 or 2 = parameter level-1 or 2

References

[1] Nakayama, W., 1996, ''Thermal Management of Electronic Equipment: Research Needs in the Mid-1990s and Beyond,'' Appl. Mech. Rev., **49**(10), Pt. 2, pp. S167–S174.
[2] Nakayama, W., 2001, ''An Approach to Fast Thermal Design of Compact Electronic Systems: A JSME Project,'' *Proc. InterPACK*, July, Kauai, HI, ASME Paper No. IPACK2001-15532.
[3] Nakayama, W., 2001, ''Emerging New Roles of CFD Simulation in Competitive Market Environment,'' *Proc. 7th THERMINIC Workshop*, September 24–27, 2001, Paris, France, pp. 223–229.
[4] Nakayama, W., 2003, ''The Build-up Approach to Combat Complexity and Uncertainties in Thermal Analysis of Compact Electronic Equipment: A JSME Project,'' *6th ASME-JSME Thermal Engineering Joint Conference*, March 16–20, 2003, Hawaii, Paper TED-AJ03-566.
[5] Vinke, H., and Lasance, C. J. M., 1997, ''Compact Models for Accurate Thermal Characterization of Electronic Parts,'' IEEE Trans. Compon., Packag. Manuf. Technol., Part A, **20**, pp. 411–419.
[6] Nakayama, W., 2000, ''Thermal Issues in Microsystems Packaging,'' IEEE Trans. Adv. Packag., **23**(4), pp. 602–607.
[7] Nakayama, W., 2003, ''A Methodology to Cope With Geometrically Complex Heat Transfer Systems; The Cases of Heat Conduction Through Composite Slabs,'' Int. J. Heat Mass Transfer, **46**, pp. 3397–3409.
[8] Taguchi, G., 1987, *Systems of Experimental Design: Engineering Methods to Optimize Quality and Minimize Cost*, UNIPUB/Kraus International, White Plains, New York (The original Japanese 3rd version was published from Maruzen, Tokyo, 1976).
[9] Kraycir, J. R., Cleverley, D. S., Levine, R. F., and Lorenzen, J. A., 1997, ''Package Manufacture,'' Chapter 6 of Microelectronics Packaging Handbook, Technology Drivers, Part I, R. R. Tummala, E. J. Rymaszewski, and A. G. Klopfenstein (eds.), Chapman & Hall, New York, pp. I-556–619.
[10] May, G. S., 2002, ''Fundamentals of Package Manufacturing,'' Chapter 20 of Fundamentals of Microsystems Packaging, R. R. Tummala (ed.), McGraw-Hill, New York, pp. 780–844.
[11] Yu, Q., Kashiwamura, T., Shiratori, M., and Yamada, T., 1999, ''Optimal and Robust Design of Nonlinear Structures Under Uncertain Loads Using Statistical Optimization Method,'' *Computer Aided Optimum Design of Structures VI*, S. Hernandez, A. J. Kassab, and C. A. Brebbia (eds.), WIT Press, Southampton, Boston, pp. 97–105.
[12] *Design Director Plus, Statistical Design Support System, User Manual*, NHK Co., Tokyo, Japan, 2001.
[13] Kirby, M., 2001, *Geometric Data Analysis*, Wiley, New York, pp. 51–61.